Engineering 4 (2018) 816–821

Contents lists available at ScienceDirect

Engineering

journal homepage: www.elsevier.com/locate/eng

Research
Precision Engineering—Article

Picosecond Laser Surface Texturing of a Stavax Steel Substrate for Wettability Control

Xincai Wang [a], Hongyu Zheng [a,b,c,*], Yinchi Wan [a], Wenhe Feng [a], Yee Cheong Lam [b]

[a] Singapore Institute of Manufacturing Technology (SIMTech), A*STAR, Singapore 138634, Singapore
[b] SIMTech-NTU Joint Laboratory (Precision Machining), Nanyang Technological University, Singapore 639798, Singapore
[c] School of Mechanical Engineering, Shandong University of Technology, Zibo 255000, China

ARTICLE INFO

Article history:
Received 24 April 2018
Revised 30 September 2018
Accepted 29 October 2018
Available online 3 November 2018

Keywords:
Picosecond laser
Surface texturing
Stavax steel
Polymer
Hydrophobicity

ABSTRACT

In this investigation, a picosecond laser was employed to fabricate surface textures on a Stavax steel substrate, which is a key material for mold fabrication in the manufacturing of various polymer products. Three main types of surface textures were fabricated on a Stavax steel substrate: periodic ripples, a two-scale hierarchical two-dimensional array of micro-bumps, and a micro-pits array with nano-ripples. The wettability of the laser-textured Stavax steel surface was converted from its original hydrophilicity into hydrophobicity and even super-hydrophobicity after exposure to air. The results clearly show that this super-hydrophobicity is mainly due to the surface textures. The ultrafast laser-induced catalytic effect may play a secondary role in modifying the surface chemistry so as to lower the surface energy. The laser-induced surface textures on the metal mold substrates were then replicated onto polypropylene substrates via the polymer injection molding process. The surface wettability of the molded polypropylene was found to be changed from the original hydrophilicity to super-hydrophobicity. This developed process holds the potential to improve the performance of fabricated plastic products in terms of wettability control and easy cleaning.

1. Introduction

Controlled modification of a material's surface wettability has been the subject of significant scientific research due to its importance for various applications, which include easy cleaning, adhesion mitigation, and microfluidic and biomedical applications. In terms of wettability, the water contact angle (WCA) and contact angle hysteresis are affected by both material surface chemistry and topology [1]. Based on the Wenzel [2] and Cassie-Baxter [3] models, the roughness of the sample surface is critical in increasing its hydrophobicity or hydrophilicity. Surface morphology is one of the key factors determining the wettability of a solid surface. Various techniques have been used for surface texturing in order to create the desired surface morphologies. These techniques can be classified into two major categories: top-down processes such as the lithographic process, the template-based method [4], plasma treatment [5,6], and the laser surface treatment process [7,8]; and bottom-up processes that mainly consist of self-assembly and self-organization processes [9,10]. As a top-down approach, laser micro- and nano-processing has been extensively investigated and is developing rapidly. Picosecond (ps) and femtosecond (fs) ultrafast lasers are the most employed tools for surface texturing. The ps or fs laser pulse-induced ablation is able to produce well-controlled two-scale micro- and nano-scale surface textures [11–13] in order to fabricate certain types of surfaces with improved surface functional properties.

Thus far, a significant amount of research has been carried out on the surface treatment and modification of various types of materials, such as metallic [11,12,14–16], semiconductor [17], and polymeric [18–20] materials, to modify their wetting properties using various lasers. The mechanisms involved in the wettability conversion of structured metallic surfaces from super-hydrophilicity to super-hydrophobicity have also been well studied [12,21–22]. The mechanism for the wettability change has been found to be dependent on the specific material to be laser beam treated. Regarding laser surface-treated stainless steel, Kietzig et al. [12] have proposed that the conversion in wettability from the original hydrophilicity to super-hydrophobicity after laser treatment is due to the accumulation of a certain amount of carbon

* Corresponding author.
E-mail address: hyzheng@SIMTech.a-star.edu.sg (H. Zheng).

https://doi.org/10.1016/j.eng.2018.10.006

onto the laser-treated surface through the dissociation of carbon dioxide (CO_2) into carbon, with the active magnetite acting as a catalyst. For copper (Cu) [21], it is the adsorption of organic materials from the surrounding environment that induces the change in wettability from hydrophilic to highly hydrophobic. For laser-textured nickel (Ni) [22], the change in wettability from hydrophilicity to super-hydrophobicity has been attributed to the accumulation of a thin layer of carbon on the laser-textured Ni surface. Stavax steel is well known to be the metal that is most commonly used to fabricate mold inserts for the large-volume production of plastic or polymer products, including microfluidic devices and consumer products. The laser-produced micro-/nano-scale surface patterns on a Stavax mold surface can be duplicated onto the molded polymer product surfaces so as to improve the product's surface functional properties such as super-hydrophobicity; this is beneficial for the production of consumer plastic products with the property of easy cleaning, among other useful properties.

In this study, ps laser surface texturing on Stavax steel was systematically investigated. Three types of surface textures were demonstrated: periodic ripples, a two-scale hierarchical two dimensional (2D) array of micro-bumps, and a micro-pits array with nano-ripples. After the laser-texturing treatment, the Stavax steel initially showed hydrophilicity with a WCA of less than 10°; it then gradually acquired high hydrophobicity, and finally acquired super-hydrophobicity with a WCA of more than 150°. This wettability conversion is considered to be due to a laser irradiation-induced change in the surface topography and chemistry through the fabrication of a two-scale hierarchical 2D surface structure and the rendering of a carbon formation, resulting in a decrease of the surface energy. Laser-induced surface textures on metal mold substrates were then replicated onto polypropylene substrates via the polymer injection molding process. The surface wettability of the molded polypropylene was found to be changed from the original hydrophilicity to super-hydrophobicity, with a WCA of more than 150°.

2. Experimental

A 5 mm thick Stavax steel plate with mirror finishing on one side was used for the laser surface texturing. The Stavax steel plate first underwent sonication cleaning with acetone and methanol. A Time-Bandwidth's Duetto ps laser system was employed in the experiments to perform the laser surface treatment. The laser had a Gaussian-profiled spatial mode (TEM_{00}) with a beam quality of $M^2 < 1.3$ (M^2 represents the degree of variation of a beam from an ideal Gaussian beam) and a beam divergence of less than 0.3 mrad. The laser wavelength was near-infrared at 1.06 μm, the output power was up to 10 W, and the laser pulse width was 10.3 ps. The pulse repetition rate could be set to a minimum value of 50 kHz and continuously tuned up to 8200 kHz. The incident laser beam was focused and manipulated by a galvo-scanner, which was equipped with a telecentric f-θ lens. The focal length of the f-θ lens was 100 mm. The linear polarized raw laser beam had a diameter of 7 mm (at $1/e^2$, which is the distance between points where the intensity falls to $1/e^2 = 0.135$ times the maximum value for a Gaussian beam), which was focused and directed onto the sample surface with a beam diameter of 25 μm. The laser machining control software that was used was able to produce various machining patterns, including lines, circular or rectangular shapes, hatched patterns, and so forth. The maximum scanning speed of the galvo-scanner was 2000 mm·s^{-1}. For the surface treatment process, the focused laser beam either raster scanned a designed pattern or performed spot-by-spot ablation with a certain pulse number on each spot. The effects of the following factors were investigated: the rate of repetition, velocity of scanning, laser power density, pass number, and pulse number on each spot. In addition, we investigated the effect of the pitch of the hatched pattern on properties of the produced surface textures such as morphology, feature size, and uniformity of the produced pattern.

After laser treatment, the sample surfaces were characterized using scanning electron microscopy (SEM). The nano-features were characterized using atomic force microscopy (AFM). The surface wettability was characterized by measuring the WCA. Using the sessile drop method, the WCA was obtained with a VCA Optima contact angle measurement system (VCA-2500XE, AST Products, Inc.). During the WCA measurement, a water droplet with a specific volume was created with a syringe connected to a capillary tip. The water droplet was then gently detached onto the substrate. The image of the droplet was recorded with a camera and analyzed with the software to determine the tangent line for the contact angle. The chemical status and elemental composition of the original and laser-treated sample surfaces were analyzed using X-ray photoelectron spectroscopy (XPS, ESCALAB 250Xi, Thermo Fisher Scientific).

3. Results and discussion

Fig. 1 schematically shows the two main types of designed patterns that were employed to produce the desired texturing. The line-hatched pattern was produced by scanning the focused laser beam along the regular hatched raster pattern, as shown in Fig. 1(a), so as to yield desired surface textures such as a micro-bumps array pattern. The dot array pattern, as shown in Fig. 1(b), was produced via dot-by-dot ablation with the laser beam so as to yield a 2D array of the micro-pits texturing pattern. In addition to the ultrafast laser-induced self-organizing effect, we investigated the dependence of the induced surface patterns on the different laser parameters, including the laser fluence, pulse repetition rate, beam-scanning velocity, pass number or pulse number on each spot, and hatching density. It was found that three types of surface texture patterns could be produced: periodic ripples, a two-scale hierarchical 2D array of micro-bumps, and a micro-pits array with nano-ripples.

First, the Stavax steel substrate was treated with the following laser parameters: The laser energy fluence was set at 1.18 J·cm^{-2}, the repetition rate was set at 1 MHz, the scanning velocity was set at 500 mm·s^{-1}, the repetition pass number was set at 30, and the hatched distance was set to be 25 μm for both directions in the hatched pattern, as shown in Fig. 1(a). A uniform surface pattern comprising a micro-bumps array was produced on the Stavax substrate with an area of 20 mm × 20 mm, as shown in Fig. 2.

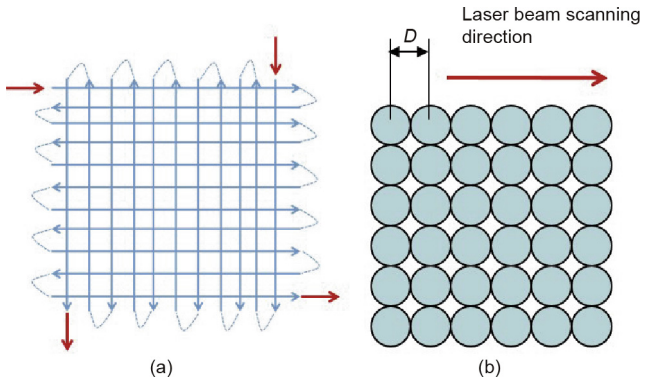

Fig. 1. Schematic of the designed laser-textured patterns. (a) Line-hatched pattern; (b) dot array pattern.

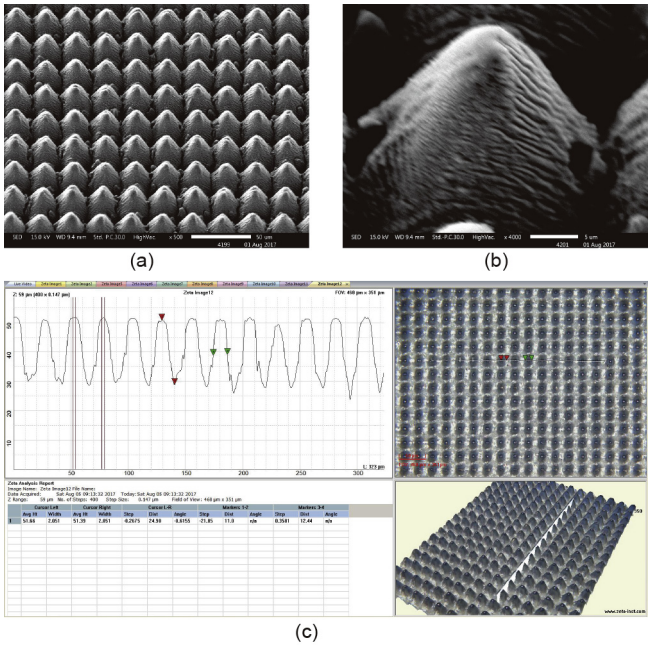

Fig. 2. Laser-produced two-scale micro-/nano-bumps array surface texturing. (a) SEM image under ×500 magnification; (b) SEM image under ×4000 magnification; (c) profile measurement.

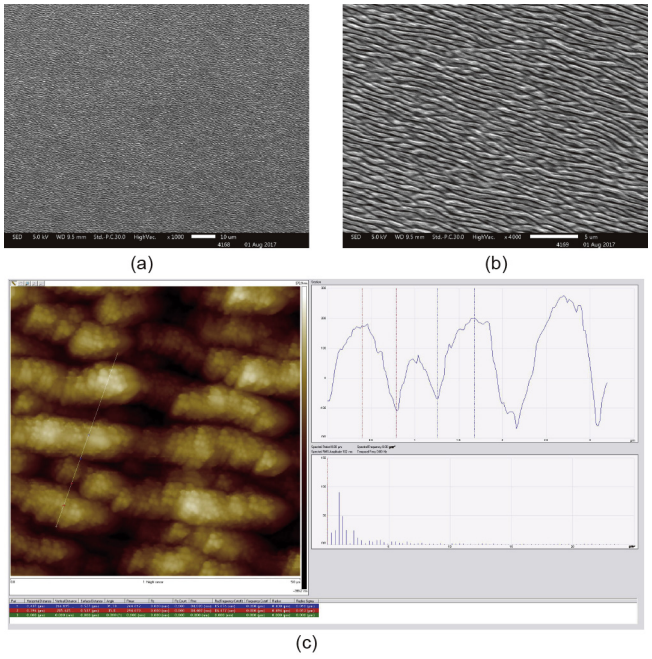

Fig. 3. Laser-produced periodic ripple surface textures on a Stavax surface. (a) SEM image under magnification of ×1000; (b) SEM image under magnification of ×4000; (c) AFM image.

The estimated processing time was 5 min. It was observed that a uniform and consistent surface pattern was produced. Fig. 2(c) illustrates the measured feature profile of the micro-bumps array surface texture. The diameter of a micro-bump was 12.5 μm, the period of the pattern was 25 μm, and the height of the micro-bumps pattern was about 21.9 μm. Fig. 2(b) shows a magnified SEM image of a micro-bump; periodic surface ripples were observed to be superimposed onto the surface of the micro-bump. The period of this ripple was 800 nm and the modulation depth was 220 nm. Thus, a two-scale hierarchical 2D surface texture based on a micro-bumps array was produced.

Next, the Stavax substrate was treated with the following laser parameters: The laser fluence was set at 0.8 J·cm^{-2}, the repetition rate was set at 1 MHz; the scanning velocity was set at 1000 mm·s^{-1}, with a pass number of 1; and the hatched distance was set to be 5 μm for both directions in the hatched pattern, as shown in Fig. 1(a). A large-area uniformly distributed periodic ripple pattern was produced with an area of 20 mm × 20 mm, as shown in Fig. 3. The estimated processing time was 3 min. Using AFM measurement, the period of the ripple was found to be 800 nm with a modulation depth of 220 nm.

Laser surface treatment was then conducted in two steps. The first step involved the dot array pattern (Fig. 1(b)) with laser parameters set as follows: a laser energy fluence of 1.43 J·cm^{-2}, a pulse repetition rate of 1 MHz, and a dot pitch of 35 μm for 5000 pulses on each location. The second step involved the line-hatching pattern (Fig. 1(a)) with laser parameters set as follows: a laser energy fluence of 0.8 J·cm^{-2}, a pulse repetition rate of 1 MHz, a scanning velocity of 1000 mm·s^{-1} for only one pass, and a hatching pitch of 5 μm for both directions in the line-hatching pattern, as shown in Fig. 1(a). A 2D pattern of a micro-pits array covered with nano-scale periodic ripples in between the pits was fabricated, as shown in Fig. 4. The micro-pit diameter was 13 μm, the pit depth was 15 μm with a pitch of 35 μm, the period of the ripple was around 800 nm, and the ripple depth was 220 nm, as measured with AFM (Fig. 4(c)). With this combined two-step process, the scanned area was 20 mm × 20 mm and the estimated total processing time was 8 min.

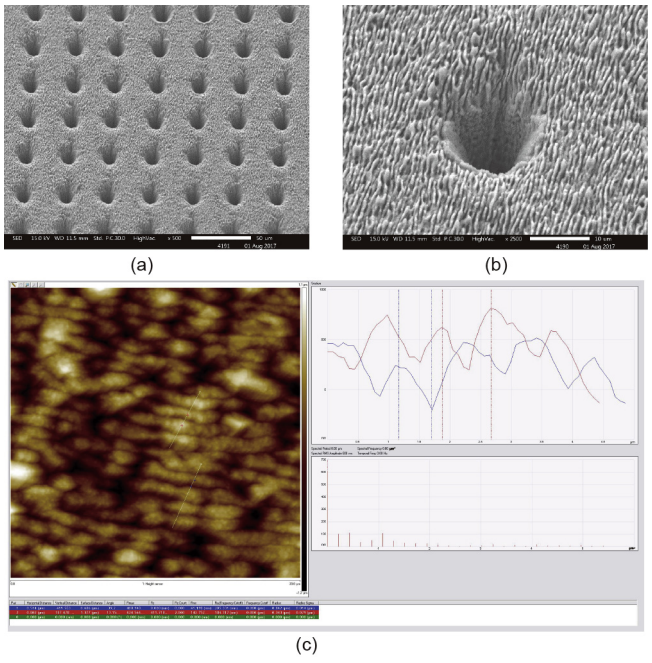

Fig. 4. Laser-produced 2D pattern of a micro-pits array covered with nano-scale periodic ripples. (a) SEM image under × 500 magnification; (b) SEM image under ×2500 magnification; (c) AFM image.

It was observed that the laser fluence used for the ripple formation was 0.8 J·cm^{-2}; this was a bit higher, albeit on the same order of magnitude, as the ablation threshold of 0.5 J·cm^{-2} that was used on stainless steel with the ps laser [23]. Previous studies [24,25] have clearly shown that when a solid surface is irradiated with a certain number of laser pulses with a laser energy fluence close to the single pulse ablation threshold, a periodic surface-modulation pattern is produced with a period that is close to the laser wavelength.

It has been suggested that the incident laser light may interfere with the scattered waves from the surface disturbance so as to create a standing wave that leads to the formation of ripples [26]. In this case, the laser energy density is higher than the threshold fluence for the periodic surface material melting following the interference pattern. The thin layer of molten material then re-solidifies immediately to form a ridged structure. A certain degree of laser power intensity is required in order for the interference pattern to be engraved or etched on the target sample surface. The sample surface is initially roughened by the first laser pulse irradiation; after that, subsequent pulses create periodic ripples via the interference effect [27]. The laser beam parameters, which include the laser wavelength, beam polarization, and incident angle of the radiation, determine the period of the ripple pattern that is produced.

Fig. 2 shows a laser-produced pattern that is a regular micro-bumps array. From the magnified SEM image, it was found that the surface of the micro-bumps was covered with nano-ripples, creating a micro-nano hierarchical 2D surface pattern. It was expected that this type of two-scale surface pattern would be able to modify the surface wettability into hydrophobicity and even super-hydrophobicity by increasing the WCA. However, it was found that the sample surface displayed super-hydrophilicity immediately after laser surface treatment, with a WCA of less than 10°. The WCA of the sample surface then gradually increased to 120° within 3 d, indicating a shift to a highly hydrophobic surface. Eventually, after 30 d, the WCA of the laser-treated Stavax sample surface increased to more than 150°, indicating that a super-hydrophobic surface had been achieved. Fig. 5 illustrates the measured WCA of the Stavax sample substrate before and after laser treatment. The WCA of the untreated Stavax steel was 73°; after laser surface texturing, the surface WCA increased to 154°. This result indicates that laser surface treatment was able to convert the original hydrophilic Stavax steel surface into a super-hydrophobic surface under specific laser parameters.

The surface wetting property of a solid substrate is determined by its surface morphological structure and surface chemistry properties. Therefore, an XPS analysis was conducted to characterize the elemental composition and chemical compositions of the Stavax substrate surface before and after laser treatment to study its surface chemistry effects. Fig. 6 illustrates the XPS survey spectra of the untreated and laser-treated Stavax steel surface. Before collecting the spectra, the samples were treated with argon ion (Ar^+) sputtering for 20 s to ensure that the surface was clean with no contaminants from the ambient atmosphere.

As shown in Fig. 6, it was observed that for untreated Stavax steel, the carbon (C) 1s peak intensity was very weak. In contrast, for laser-treated Stavax steel, the C 1s peak intensity was much higher. The increment of the relative C 1s peak intensity indicated that the elemental concentration of C on the laser-textured Stavax steel surface had increased. Based on the relative intensities of elements in the XPS spectra, the elemental concentrations (at%) of C, oxygen (O), iron (Fe), and chromium (Cr) on the untreated and laser-treated steel substrate surfaces were derived (Table 1). It was found that the C concentration on the laser-treated Stavax steel surface had increased from 9.6 at% on the untreated Stavax steel surface to 29.7 at%. Therefore, we believe that a thin layer of nonpolar carbon had accumulated on the laser-treated Stavax steel surface. The dissociation of CO_2 into carbon is considered to be the main reason for the carbon layer formation. The dissociative reaction of CO_2 was initiated by active magnetite $Fe_3O_{4-\delta}$ ($0 < \delta < 1$), an oxygen-deficient iron oxide that may have been induced by the ultrafast laser surface treatment [12,15]. We believe that this nonstoichiometric magnetite $Fe_3O_{4-\delta}$ ($0 < \delta < 1$) acted as a catalyst to initiate the dissociative adsorption of CO_2 [28–30], producing carbon monoxide and carbon as the outcome of the CO_2 dissociation, and moving oxygen anions into lattice vacancies of the steel alloy to form stoichiometric Fe_3O_4. Therefore,

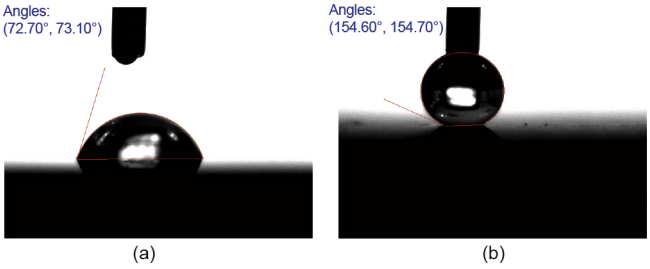

Fig. 5. The WCA of the (a) untreated and (b) laser-treated Stavax substrate surface.

Table 1
Concentrations of the elements C, O, Fe, and Cr (at%).

Element	Untreated Stavax steel	Laser-treated Stavax steel
C	9.6	29.7
O	43.5	48.4
Fe	27.1	15.3
Cr	19.8	6.7

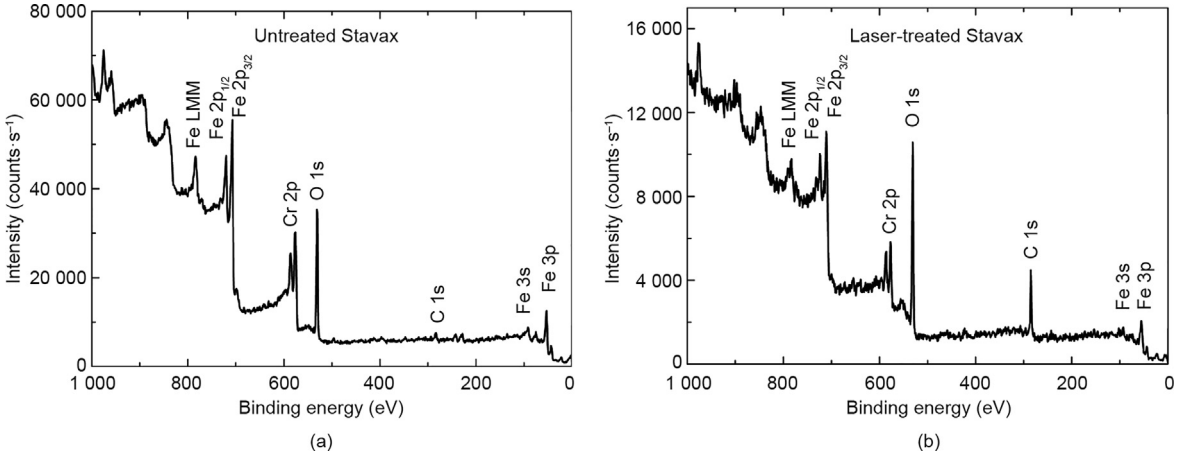

Fig. 6. XPS spectra of the (a) untreated and (b) laser-treated Stavax substrate surface.

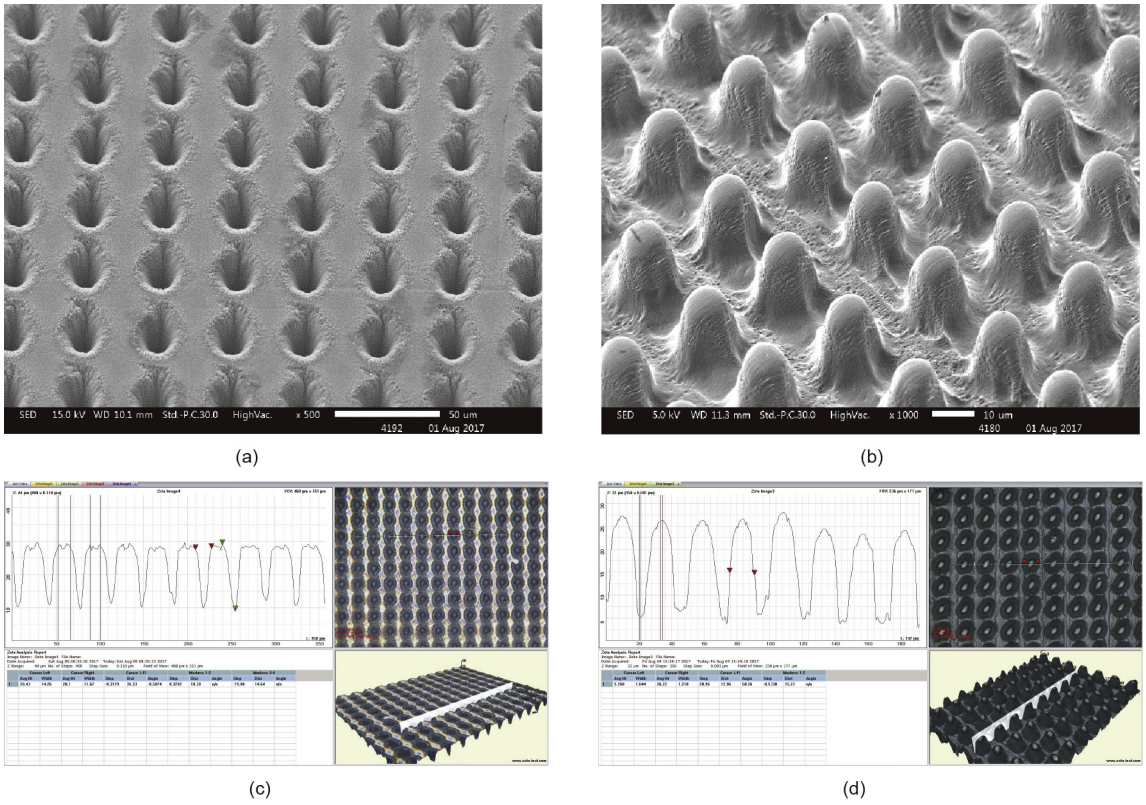

Fig. 7. SEM images on (a) a laser-textured Stavax steel surface and (b) a molded polypropylene surface; measured surface profiles on (c) laser-textured Stavax steel and (d) molded polypropylene.

a nonpolar amorphous carbon accumulation layer formed on the laser-treated Stavax steel surface due to the CO_2 decomposition reaction. This amorphous carbon layer has a low surface energy. Thus, the combination of the CO_2 decomposition reaction and the laser-induced two-scale hierarchical 2D surface texture (Fig. 2) resulted in the formation of a super-hydrophobic Stavax steel surface with a WCA greater than 150°.

Next, the laser-induced micro-pits array surface pattern on the metal mold substrate was replicated onto a polypropylene substrate via the polymer injection molding process. Fig. 7(a) shows the laser-produced surface textures on the Stavax steel substrate. From the three-dimensional profile measurement shown in Fig. 7(c), it can be seen that the micro-pit diameter is 15 μm, the period of the pits is 30 μm, and the depth of the pits is 17 μm. With the polymer injection molding process, the micro-pits array pattern on the Stavax steel mold was converted into a micro-bumps array pattern on the polypropylene substrate, as shown in Fig. 7(b). The molded micro-bump diameter was about 15 μm, the period was 30 μm, and the bump height was about 20 μm, as shown in Fig. 7(d). Fig. 8 shows the measured WCA for the original and for the molded and textured polypropylene substrate. It was found that the WCA increased from 96° for the original polypropylene to 156° for the injection-molded textured polypropylene. This increase of 60° indicates that a super-hydrophobic polypropylene surface was achieved.

It was observed that due to the formation of the 2D array of micro-bumps surface structures, as shown in Fig. 7(b), when the water droplet comes into contact with the laser-textured surface, the water droplet may not be able to fully wet the whole surface area; rather, it may stay on top of the micro-bumps, causing some air to be entrapped between the water droplet and the textured bottom surface, and resulting in a composite interface. Following the Cassie-Baxter [3] model, this may be the cause of the WCA increasing to more than 150°, as shown in Fig. 8(b).

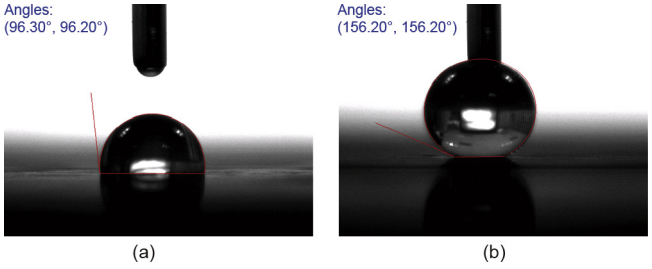

Fig. 8. WCA of (a) original and (b) molded textured polypropylene surface.

4. Conclusions

In conclusion, a systematic investigation of the ps laser surface texturing of a Stavax steel substrate was conducted. Three types of surface textures were achieved: periodic ripples, a two-scale hierarchical 2D array of micro-bumps, and a micro-pits array with nano-ripples. After laser surface treatment, the Stavax surface showed super-hydrophobicity with a WCA of more than 150°. The XPS analysis indicated that a nonpolar amorphous low-surface-energy carbon layer accumulated on the laser-treated Stavax steel surface via the CO_2 decomposition reaction. The combination of the CO_2 decomposition reaction and the laser-induced two-scale roughness structure produced a super-hydrophobic Stavax steel surface. Furthermore, the laser-induced surface textures on the metal mold substrate were replicated onto a polypropylene substrate via the polymer injection molding process. The results showed that the laser-induced surface textures were successfully duplicated onto the polypropylene surface. The WCA of the molded textured polypropylene surface changed from the original 96° to

156°, indicating that a super-hydrophobic polypropylene surface was achieved. This developed process holds potential for application in the fabrication of microfluidic devices and consumer plastic products with an easy cleaning function.

Acknowledgements

The authors would like to thank Ms. Hong Xie for her help with XPS measurement. They would also like to thank the Agency for Science, Technology and Research (A*STAR) of Singapore for financial support.

Compliance with ethics guidelines

Xincai Wang, Hongyu Zheng, Yinchi Wan, Wenhe Feng, and Yee Cheong Lam declare that they have no conflict of interest or financial conflicts to disclose.

References

[1] Johnson RE Jr, Dettre RH, Brandreth DA. Dynamic contact angles and contact-angle hysteresis. J Colloid Interface Sci 1977;62(2):205–12.
[2] Wenzel RN. Surface roughness and contact angle. J Phys Colloid Chem 1949;53(9):1466–7.
[3] Cassie BD, Baxter S. Wettability of porous surfaces. Trans Faraday Soc 1944;40:546–50.
[4] Li J, Fu J, Cong Y, Wu Y, Xue LJ, Han YC. Macroporous fluoropolymeric films templated by silica colloidal assembly: a possible route to super-hydrophobic surfaces. Appl Surf Sci 2006;252(6):2229–34.
[5] Kim SH, Kim JH, Kang BK, Uhm HS. Superhydrophobic CF_x coating via in-line atmospheric RF plasma of He-CF_4-H_2. Langmuir 2005;21(26):12213–7.
[6] Teshima K, Sugimura H, Inoue Y, Takai O, Takano A. Transparent ultra water-repellent poly(ethylene terephthalate) substrates fabricated by oxygen plasma treatment and subsequent hydrophobic coating. Appl Surf Sci 2005;244(1–4):619–22.
[7] Wagterveld RM, Berendsen CWJ, Bouaidat S, Jonsmann J. Ultralow hysteresis superhydrophobic surfaces by excimer laser modification of SU-8. Langmuir 2006;22(26):10904–8.
[8] Wong W, Chan K, Yeung KW, Lau KS. Surface structuring of poly(ethylene terephthalate) by UV excimer laser. J Mater Process Technol 2003;132(1–3):114–8.
[9] Kulinich SA, Farzaneh M. Hydrophobic properties of surfaces coated with fluoroalkylsiloxane and alkylsiloxane monolayers. Surf Sci 2004;573(3):379–90.
[10] Schondelmaier D, Cramm S, Klingeler R, Morenzin J, Zilkens C, Eberhardt W. Orientation and self-assembly of hydrophobic fluoroalkylsilanes. Langmuir 2002;18(16):6242–5.
[11] Vorobyev Y, Guo CL. Multifunctional surfaces produced by femtosecond laser pulses. J Appl Phys 2015;117(3):033103.
[12] Kietzig AM, Hatzikiriakos SG, Englezos P. Patterned superhydrophobic metallic surfaces. Langmuir 2009;25(8):4821–7.
[13] Wu PH, Cheng CW, Chang CP, Wu TM, Wang JK. Fabrication of large-area hydrophobic surfaces with femtosecond-laser-structured molds. J Micromech Microeng 2011;21(11):115032.
[14] Tang M, Shim V, Pan ZY, Choo YS, Hong MH. Laser ablation of metal substrates for super-hydrophobic effect. J Laser Micro Nanoeng 2011;6(1):6–9.
[15] Kietzig AM, Mirvakili MN, Kamal S, Englezos P, Hatzikiriakos SG. Laser-patterned super-hydrophobic pure metallic substrates: Cassie to Wenzel wetting transitions. J Adhes Sci Technol 2011;25:2789–809.
[16] Moradi S, Kamal S, Englezos P, Hatzikiriakos SG. Femtosecond laser irradiation of metallic surfaces: effects of laser parameters on superhydrophobicity. Nanotechnology 2013;24(41):415302.
[17] Her TH, Finlay RJ, Wu C, Deliwala S, Mazur E. Microstructuring of silicon with femtosecond laser pulses. Appl Phys Lett 1998;73(12):1673–5.
[18] Wang B, Wang X, Zheng H, Lam YC. Surface wettability modification of cyclic olefin polymer by direct femtosecond laser irradiation. Nanomaterials 2015;5(3):1442–53.
[19] Toosi SF, Moradi S, Kamal S, Hatzikiriakos SG. Superhydrophobic laser ablated PTFE substrates. Appl Surf Sci 2015;349:715–23.
[20] Li ZL, Chu PL, Zheng HY, Lim GC. Process development of laser machining of carbon fibre reinforced plastic composites. In: Proceedings of the International Congress on Applications of Lasers & Electro-Optics (ICALEO); 2008 Oct 20–23; Temecula, CA, USA; 2008.
[21] Long J, Zhong M, Fan P, Gong D, Zhang H. Wettability conversion of ultrafast laser structured copper surface. J Laser Appl 2015;27(S2):S29107.
[22] Wang XC, Wang B, Xie H, Zheng HY, Lam YC. Picosecond laser micro/nano surface texturing of nickel for superhydrophobicity. J Phys D Appl Phys 2018;51(11):115305.
[23] Račiukaitis G, Brikas M, Gečys P, Voisiat B, Gedvilas M. Use of high repetition rate and high power lasers in microfabrication: how to keep the efficiency high? J Laser Micro Nanoeng 2009;4(3):186–91.
[24] Zhou GS, Fauchet PM, Siegman AE. Growth of spontaneous periodic surface-structures on solids during laser illumination. Phys Rev B Condens Matter 1982;26(10):5366–81.
[25] Preston JS, Sipe JE, Sipe JE, van Driel HM. Pattern formation during laser melting of silicon. Phys Rev B Condens Matter 1989;40(6):3942–54.
[26] Isenor NR. CO_2 laser-produced ripple patterns on Ni_xP_{1-x} surfaces. Appl Phys Lett 1977;31:148–50.
[27] Miller JC, Haglund RFJ, editors. Laser ablation and desorption. Amsterdam: Elsevier Inc.; 1997.
[28] Tamaura Y, Tabata M. Complete reduction of carbon dioxide to carbon using cation-excess magnetite. Nature 1990;346(6281):255–6.
[29] Zhang CL, Li S, Wang LJ, Wu TH, Peng SY. Studies on the decomposition of carbon dioxide into carbon with oxygen-deficient magnetite: I. preparation, characterization of magnetite, and its activity of decomposing carbon dioxide. Mater Chem Phys 2000;62(1):44–51.
[30] Zhang CL, Li S, Wang LJ, Wu TH, Peng SY. Studies on the decomposing carbon dioxide into carbon with oxygen-deficient magnetite: II. the effects of properties of magnetite on activity of decomposition CO_2 and mechanism of the reaction. Mater Chem Phys 2000;62(1):52–61.